Research Article

Robust Design of S-Shaped Box Beams Subjected to Compressive Load

A. Khakhali,[1] A. Darvizeh,[1] A. Masoumi,[2] N. Nariman-Zadeh,[1, 3] and A. Shiri[1]

[1] *Department of Mechanical Engineering, Faculty of Engineering, The University of Guilan,*
 P.O. Box 3756, Rasht 3756, Iran
[2] *Schools of Mechanical Engineering, Faculty of Engineering, University of Tehran, Tehran, Iran*
[3] *Intelligent-Based Experimental Mechanics Center of Excellence, School of Mechanical Engineering,*
 Faculty of Engineering, University of Tehran, Tehran, Iran

Correspondence should be addressed to A. Khakhali, abolfazl.khalkhali@gmail.com

In order to design the automotive components considering probabilistic uncertainties in the decision variables, it is desired to perform a robust design process. The peak crushing force of the energy absorber components is one of the important objectives of the design of such components. In this paper, at first, the peak crushing force of the S-shaped box beams, as a highly simplified model of front member of a vehicle body, is extracted mathematically. Using such obtained mathematical model and Monte Carlo simulation, genetic algorithm is then used for the robust design of the S-shaped box beams having probabilistic uncertainties in material and geometrical parameters. In this way the variance-per-mean ratio of the peak crushing force (P_{max}) is considered as the objective function. It is shown that some interesting relationships as useful robust design principles involved in the performance of the S-shaped box beams can be discovered by the robust design of the obtained mathematical model.

1. Introduction

Higher-speed transportation increases the probability of traffic accidents which in turn cause serious damages to passengers. Design of auxiliary metal structure or structural components capable of sustaining prescribed loads and absorbing crushing energies during plastic deformation has become a special task in design to ensure the occupant safety. Therefore the crash characteristic of energy absorbing component has received considerable attention over the past decades [1–7]. As a highly simplified model of the front-side member of a

vehicle body, which plays an important role in absorbing energy during collision, various investigators in previous works [8–14] have studied the crushing behavior of the S-shaped structures.

In real engineering practices, there exist various sources of uncertainty which have to be compensated through optimal robust design approach [15–17]. Those uncertainties include model parameter variations due to environmental conditions, incomplete knowledge of parameters including material and geometry variables, age, and so forth [18–20]. In conventional optimum system design, uncertainties are not addressed and the optimization process is accomplished deterministically. In fact, it has been shown that optimization without considering uncertainty generally leads to nonoptimal and potentially high-risk solution [15, 21–25]. Therefore, it is very desirable to find a robust design whose performance variation in the presence of uncertainties is not high. Generally, there exist two approaches addressing the stochastic robustness issue, namely, robust design optimization (RDO) and reliability-based design optimization (RBDO) [26]. Both approaches represent nondeterministic optimization formulations in which the probabilistic uncertainty is incorporated into the robust optimal design process. Therefore, the propagation of a prior knowledge regarding the uncertain parameters through the system provides some probabilistic metrics such as random variable and random process [21]. In RDO approach, the robust performance is required to be less sensitive to the random variation induced by uncertain parameters so that the performance degradation from ideal deterministic behavior is minimized. In RBDO approach, some evaluated reliability metrics subjected to probabilistic constraints are satisfied so that the violation of design requirement is minimized. Regardless of the choice of any of these two approaches, the objective function (e.g., peak crushing force) and the constraints of the optimal design should be evaluated reflecting the effect of probabilistic nature of uncertain parameters in the performance of the system. With the aid of ever-increasing computational power, there have been a great amount of research activities in the field of robust analysis and design devoted to the use of Monte Carlo simulation [21, 22]. In fact, MCS has also been used to verify the results of other methods in RDO or RBDO problems when sufficient number of sampling is adopted. In the Monte Carlo simulation (MCS) method, random samples are generated assuming pre-defined probabilistic distributions for uncertain parameters.

Basically, the optimization process is defined as finding a set of values for a vector of design variables so that it leads to an optimum value of an objective or cost function. In such single-objective optimization problems, there may or may not exist some constraint functions on the design variables and they are, respectively, referred to as constrained or unconstrained optimization problems. There are many calculus-based methods including gradient approaches to search for mostly local optimum solutions and these are well documented [27, 28]. However, some basic difficulties in the gradient methods such as their strong dependence on the initial guess can cause them to find a local optimum rather than a global one. This has led to other heuristic optimization methods, particularly Genetic Algorithms (GAs) that are being used extensively during the last decade [29, 30]. Such nature-inspired evolutionary algorithms differ from other traditional calculus-based techniques [31, 32]. The main difference is that GAs work with a population of candidate solutions and not with a single solution in the search space. This helps significantly to avoid being trapped in local optima [33] as long as the diversity of the population is well preserved.

In this paper, peak crushing force of the S-shaped box beams is mathematically modeled. The obtained model is then used in a combined robust and reliability-based design approach to find a reliable and robust design. In this way, to minimize the variation of
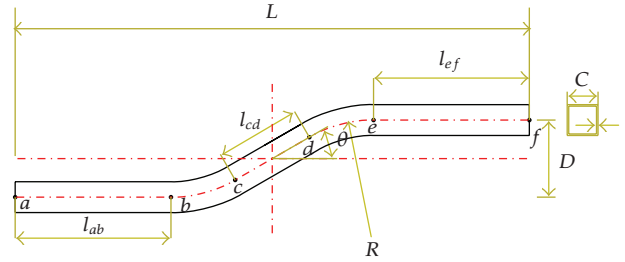
Figure 1: The geometric parameters of S-shaped box beams.

the peak crushing force ($P_{\max}$) subjected to probabilistic constraint, genetic algorithm is used. In this single-objective GA optimization problem, variance-per-mean ratio of $P_{\max}$ is considered as objective function and for each generation the value of mean and variance of objective function and the value of probability of failure are calculated using the Monte Carlo simulation (MSC) method. The value of energy absorption of each obtained design point under specific load and boundary conditions is then carried out using finite-element commercial software ABAQUS/Explicit. Results are informative and maybe effectively used for the design of S-shaped square tubes.

2. Extraction of Peak Crushing Force

The front- and rear-side members of vehicle, which play an important role in absorbing energy during collision, usually have a curved shape to avoid interference with other components like engine, driving system and fuel tank, and so forth. The S-shaped box beam which is an idealized model of front-side member of a vehicle body is depicted in Figure 1. Any variation of geometric parameters which are denoted as curve radius (R), curve angle (θ), web width (C), wall thickness (t), and offset of two-end part (D) will lead to new design and new behavior. In this study, the total length of the structure L is fixed equal to 1 m. It should be noted that both the straight lengths (l_{ab} and l_{ef}) and oblique length (l_{cd}) are derived variables, depending on the values of the curve angle and curve radius. The mechanical properties of employed material can be specified with independent parameters, namely, elastic modulus (E), Poisson's ratio (v), yielding stress (σ_0), and density (ρ).

Due to geometrical restriction, the upper bound of curve radius depends on the offset of the two-end part (D) and the curve angle (θ) and is given by

$$R_{\max} = \frac{D}{2(1 - \cos\theta)}. \tag{2.1}$$

Loading conditions considered in the mathematical model are depicted in Figure 2. The front end of the beam is considered free just in the direction of the external load, and the rear end has been fully clamped. Free-body diagram of the S-beam under the applied load P is depicted in Figure 3; Q_a, P_f, and Q_f are the reaction forces, and M_a and M_f are the reaction moments.
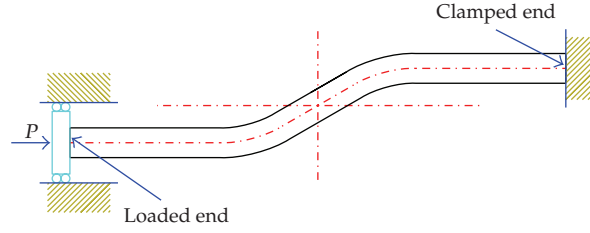
Figure 2: Loading conditions considered in the mathematical model.

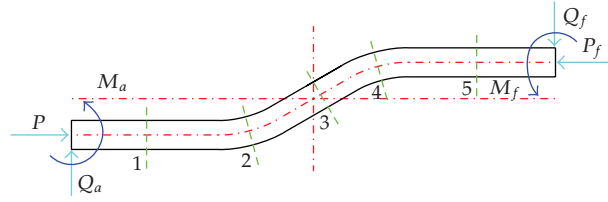**Figure 3:** Free-body diagram of the S-beam under the applied load.

The equilibrium equations for the S-beam are expressed as follows:

$$P_f = P,$$
$$Q_a = Q_f = Q,$$

(2.2)

$$M_f = -M_a - PD + QL.$$

(2.3)

For determining unknown reactions, two additional equations are needed. Equations for the deflection along direction y and the slope of beam at the point a can be used to solve this indeterminate system. Using Castigliano's theorem, these equations can be written as follows:

$$y_a = \frac{\partial U}{\partial Q_a} = 0,$$

(2.4)

$$\theta_a = \frac{\partial U}{\partial M_a} = 0,$$

(2.5)

where U is the strain energy of the beam under the applied load P. For simplicity, in this study, only the strain energy due to bending has been considered and formulated as follows:

$$U = \int \frac{M_s^2}{2EI} ds,$$

(2.6)

where, M_s is the cross-sectional bending moment along the beam. To determine M_s, the five different sections depicted in Figure 3 along the beam have been considered. The equation of the equilibrium of moment for these sections is expressed as follows For Section 1.

$$M_1 = M_a - Q_a x_1, \tag{2.7}$$

where x_1 is the distance from a along the first straight part ab.

For Section 2,

$$M_2 = M_a + PR(1 - \cos\theta_1) - Q_a(l_{ab} + R\sin\theta_1), \tag{2.8}$$

where θ_1 denotes meridian coordinate system along the first curve part bc.

For Section 3,

$$M_3 = M_a + P(R(1 - \cos\theta) + x_2\sin\theta) - Q_a((l_{ab} + R\sin\theta) + x_2\cos\theta), \tag{2.9}$$

where x_2 is the distance from c along the oblique part cd.

For Section 4,

$$M_4 = M_a + P[R(1 - \cos\theta) + l_{cd}\sin\theta + R(\cos(\theta - \theta_2) - \cos\theta)) \\ - Q_a[(l_{ab} + R\sin\theta) + l_{cd}\cos\theta + R(\sin\theta - \sin(\theta - \theta_2))], \tag{2.10}$$

where θ_2 denotes the meridian coordinate system along the second curve part de.

For Section 5,

$$M_5 = -M_f + Q_f x_3, \tag{2.11}$$

where x_3 is the distance from f along the second straight part ef. Substituting (2.6)–(2.11) and (2.3) in (2.4),

$$y_a = \frac{\partial U}{\partial Q_a} = \sum_{i=1}^{5} \int \frac{M_i}{EI} \frac{\partial M_i}{\partial Q_a} ds$$

$$= -\frac{1}{EI}\left(\int_0^{l_{ab}} M_1 x_1 dx_1 + \int_0^{\theta} M_2(l_{ab} + R\sin\theta_1)Rd\theta_1 \right.$$

$$+ \int_0^{l_{cd}} M_3((l_{ab} + R\sin\theta) + x_2\cos\theta)dx_2 \tag{2.12}$$

$$+ \int_0^{\theta} M_4(l_{ab} + 2R\sin\theta + l_{cd}\cos\theta - R\sin(\theta - \theta_2))Rd\theta_2$$

$$\left. + \int_0^{l_{ef}} (M + PD - Q(L - x_3))(L - x_3)dx_3 \right),$$

which can be evaluated as

$$f M_a - g Q_a + h P = 0, \tag{2.13}$$

where

$$f = \frac{l_{ab}^2}{2} + R(l_{ab}\theta + R(1 - \cos\theta)) + \left((l_{ab} + R\sin\theta)l_{cd} + \frac{l_{ab}^2}{2}\cos\theta \right)$$

$$+ R((l_{ab} + 2R\sin\theta + l_{cd}\cos\theta)\theta - R(1 - \cos\theta)) + Ll_{ef}^3 - \frac{l_{ef}^2}{2},$$

$$g = \frac{l_{ab}^3}{3} + R\left(l_{ab}^2\theta + \frac{R^2}{2}(1 - \cos 2\theta) + 2l_{ab}R(1 - \cos\theta) \right)$$

$$+ \left((l_{ab} + R\sin\theta)^2 l_{cd} + \frac{l_{ef}^3}{3}\cos\theta + 2(l_{ab} + R\sin\theta)\cos\theta\frac{l_{cd}^2}{2} \right)$$

$$+ R\left((l_{ab}+2R\sin\theta+l_{cd}\cos\theta)^2\theta + \frac{R^2}{2}(1 - \cos 2\theta) - 2(l_{ab}+2R\sin\theta+l_{cd}\cos\theta)R(1 - \cos\theta) \right)$$

$$+ Ll_{cd}^3 - \frac{l_{cd}^2}{2},$$

$$h = R^2(l_{ab}(\theta - \sin\theta) + R(1 - \cos\theta)) + R(1 - \cos\theta)(l_{ab} + R\sin\theta)l_{cd} + \frac{l_{cd}^3}{6}\sin 2\theta$$

$$+ \frac{l_{cd}^2}{2}((\sin\theta(l_{ab} + R\sin\theta)) + R\cos\theta(1 - \cos\theta))$$

$$+ (R(1 - 2\cos\theta) + l_{cd}\sin\theta)((l_{ab} + 2R\sin\theta) + l_{cd}\cos\theta)R\theta - \frac{R^3}{4}(1 - \cos 2\theta)$$

$$+ R^2(l_{ab} + 2R\sin\theta + l_{cd}\cos\theta)\sin\theta - R^2(R(1 - 2\cos\theta) + l_{cd}\sin\theta)(1 - \cos\theta) + D\frac{l_{ef}^2}{2}. \tag{2.14}$$

Similarly, substituting (2.6)–(2.11) and (2.3) in (2.5) gives

$$\theta_a = \frac{\partial U}{\partial M_a} = \sum_{i=1}^{5} \int \frac{M_i}{EI}\frac{\partial M_i}{\partial M_a}ds$$

$$= -\frac{1}{EI}\left(\int_0^{l_{ab}} M_1 dx_1 + \int_0^\theta M_2 R d\theta_1 + \int_0^{l_{cd}} M_3 dx_2 \right. \tag{2.15}$$

$$\left. + \int_0^\theta M_4 R d\theta_2 + \int_0^{l_{ef}} (M_a + PD - Q(L - x))dx_3 \right),$$

which can be evaluated as

$$f'M_a - g'Q_a + h'P = 0, \tag{2.16}$$

where

$$f' = l_{ab} + 2R\theta + l_{cd} + l_{ef},$$

$$g' = \frac{l_{ab}^2}{2} + R(l_{ab}\theta + R(1 - \cos\theta)) + \left((l_{ab} + \sin\theta)l_{cd} + \frac{l_{cd}^2}{2}\sin\theta\right)$$

$$+ ((l_{ab} + 2R\sin\theta + l_{cd}\cos\theta)\theta - (1 - \cos\theta)) + \frac{l_{ef}^2}{2},$$

$$h' = R^2(\theta - \sin\theta) + R(1 - \cos\theta)l_{cd} + \frac{l_{cd}^2}{2}\cos\theta + (R(1 - 2\cos\theta) + l_{cd}\sin\theta)\theta + R\sin\theta + Dl_{ef}. \tag{2.17}$$

From (2.13) and (2.16), Q_a and M_a can be obtained from

$$Q_a = J_a \times P, \tag{2.18}$$

$$M_a = K_a \times P, \tag{2.19}$$

where

$$K_a = \frac{gh' - g'h}{g'f - gf'}, \qquad J_a = \frac{fh' - f'h}{g'f - gf'}. \tag{2.20}$$

Substituting values of M_a and Q_a obtained from (2.18) and (2.19) in the (2.7)–(2.11), bending moment will be determined for any section along the beam. Similarly, the equilibrium equation of the axial force for sections shown in Figure 3 can be written as follows:

$$N_1 = P, \tag{2.21}$$

$$N_2 = P\cos\theta_1 + Q_a\sin\theta_1, \tag{2.22}$$

$$N_3 = P\cos\theta_0 + Q_a\sin\theta_0, \tag{2.23}$$

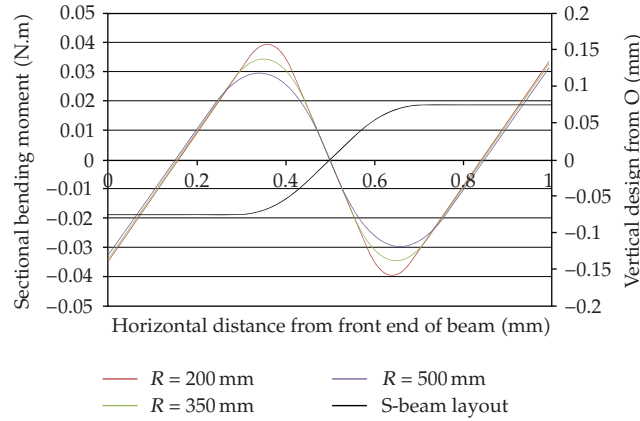$$N_4 = P\cos\theta_2 + Q_a\sin\theta_2, \tag{2.24}$$

Figure 4: Cross sectional bending moment diagram for the S-shaped box beams with three different curve radii.
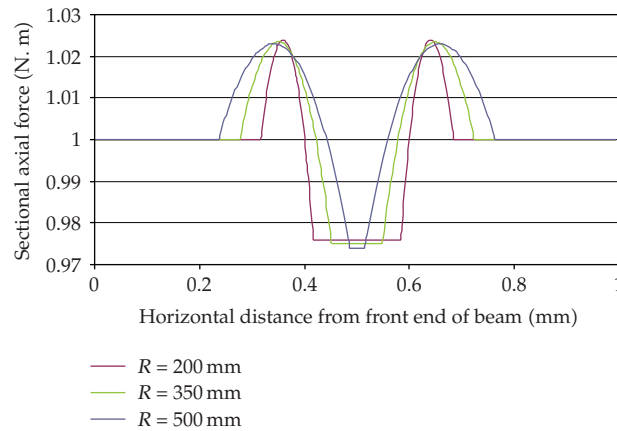

Figure 5: Cross sectional axial force diagram for the S-shaped box beams with three different curve radii.

$$N_5 = P, \tag{2.25}$$

where N_1 to N_5 are the cross-sectional axial forces of Sections 1 to 5. Figures 4 and 5 show the diagram of cross sectional bending moment and cross sectional axial force for the S-shaped box beams with geometrical parameters: $D = 150$ mm, $\theta = 30°$, and curve radii $R = 200$, 350, and 500 mm, where $P = 1$ N.

The stress at the extreme fibers of all beam sections can be determined simply from,

$$\sigma = \frac{2MC}{I} + \frac{N}{A}, \tag{2.26}$$

where I, A, and C are the inertia moment, area, and width of cross-section, respectively. Distribution of the stress σ along the beam is depicted in Figure 6. It is evident from this figure that the maximum stress locates on four places: two points at the curve parts and two points at the front- and rear-end of the beam. These locations are depicted with the points
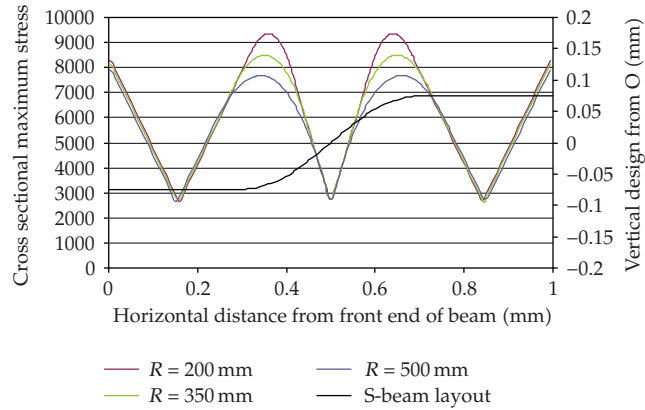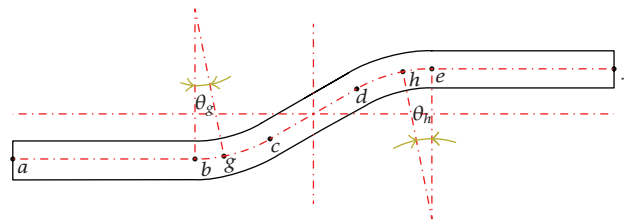
Figure 6: Distribution of the maximum stress σ along the beam.

Figure 7: The location of points a, g, h, and f.

a, g, h, and f in Figure 7, schematically. Substituting (2.18) and (2.19) in (2.8) and (2.23), the axial force and bending moment at the point g can be obtained from

$$N_g = L_g P,$$
$$M_g = K_g P, \tag{2.27}$$

where

$$L_g = \cos\theta_g + J_a \times \sin\theta_g,$$
$$K_g = K_a + R(1 - \cos\theta_g) - J_a(l_{ab} + R\sin\theta_g). \tag{2.28}$$

When the external load P is applied, the S-beam deforms elastically until yield is reached in the extreme fibers on the most stressed sections. Assuming that the beam is made of elastic-perfectly plastic material, increasing the external load, the plastic region in the cross section will be increased. In the limit, the whole section becomes plastic and then $P = P_{max}$; P_{max} which is the collapse load is also called peak crushing load.

The stress distribution across the section of a fully plastic cross section is depicted in Figure 8. Based on this figure, where c denotes the deviation of the neutral axis of the
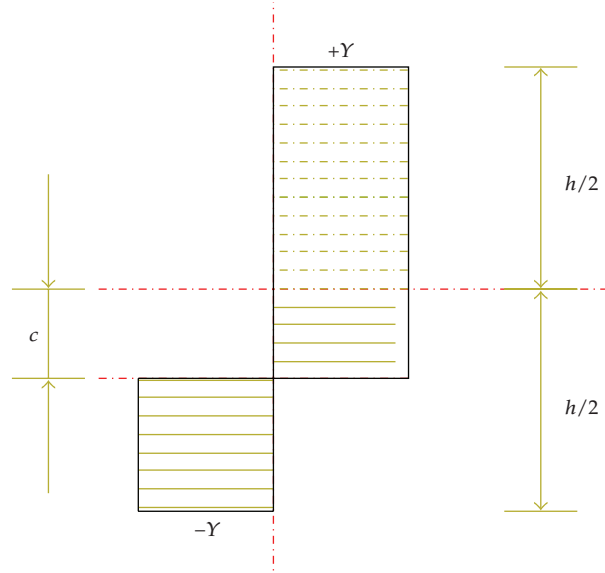
Figure 8: The stress distribution across the section of a fully plastic cross section.

longitudinal stress from the central axis of the beam, the bending moment and axial force are related to c by

$$M = \int_A \sigma x dA = YtC^2 + 2Yt\left(\left(\frac{C}{2}\right)^2 - c\right),$$

$$N = \int_A \sigma dA = 4Ytc,$$

(2.29)

where Y is the yielding stress of the material. Eliminating c from the two expressions of (2.29) leads to

$$\frac{M}{M_0} + \frac{4}{3}\left(\frac{N}{N_0}\right)^2 = 1,$$

(2.30)

where N_0 and M_0 are the fully plastic bending moment and fully plastic axial force, respectively, and can be obtained from

$$M_0 = 1,5YtC^2,$$

$$N_0 = 4YtC.$$

(2.31)

Considering sections a and f depicted in Figure 7 as the most stressed sections and substituting (2.18) in (2.30), $P_{\max}$ can be obtained from

$$P_{\max,1} = \frac{4/3}{(K_a/M_0) + (4L_a/3N_0)}. \tag{2.32}$$

Otherwise, considering sections g and h as the most stressed sections and substituting (2.18) in (2.30), $P_{\max}$ can be obtained from

$$P_{\max,2} = \frac{4/3}{(K_g M_0) + (4L_g/3N_0)}. \tag{2.33}$$

Therefore, the peak crushing force of S-shaped box beams can be obtained from

$$P_{\max} = \min\{P_{\max,1}, P_{\max,2}\}. \tag{2.34}$$

3. Stochastic Robust Analysis

In the robust design approach, it is desired to minimize the variability of a random process due to the uncertain probabilistic parameters about a deterministic behavior. Therefore, the conventional robust optimization problem can be formulated as follows:

$$\begin{aligned}
\text{Minimize} \quad & \{\mu[f(\mathbf{x}, \mathbf{d}, \mathbf{p})], \upsilon[f(\mathbf{x}, \mathbf{d}, \mathbf{p})]\}, \\
& \mathbf{x}^{(L)} \leq \mathbf{x} \leq \mathbf{x}^{(U)}, \\
& \mathbf{d}^{(L)} \leq \mathbf{d} \leq \mathbf{d}^{(U)},
\end{aligned} \tag{3.1}$$

where $f(\mathbf{x}, \mathbf{d}, \mathbf{p})$ is the performance or the cost function, μ is the mean value, and υ is one of the dispersion measure operators such as variance (σ^2), standard deviation (σ), or coefficient of variation ($C_\upsilon = \sigma/\mu$). In this study, $\mathbf{x}$ is the vector of design variables which are uncertain, $\mathbf{d}$ is the vector of deterministic design variables, and $\mathbf{p}$ is the vector of uncertain parameters which are not design variables.

In the reliability-based design approach, it is required to define some reliability metrics via some inequality constraints. Let us consider a deterministic constraint of the form $g_i(x,d,p) \leq \widehat{g}_i$, where $\widehat{g}_i$ is the limiting value of the ith constraint. This constraint can be transformed into a probabilistic constraint using the definition of a random process

$$G_i(\mathbf{x}, \mathbf{d}, \mathbf{p}) \equiv \widehat{g}_i - g_i(\mathbf{x}, \mathbf{d}, \mathbf{p}). \tag{3.2}$$

The typical probability constraint is then represented as

$$P_f^i = P[G_i(\mathbf{x}, \mathbf{d}, \mathbf{p}) \leq 0] \leq \varepsilon_i \quad (i = 1, 2, 3, \dots, m), \tag{3.3}$$

where P_f^i denotes the probability of failure of the ith reliability measure and m is the number of inequality constraints (i.e., limit-state functions) and ε_i is the highest value of the desired admissible probability of failure. It is clear that the ideal value of each P_f^i is zero.

In the reliability-based robust design process presented in this paper, an approach that simultaneously considers reliability and robustness is proposed. This methodology can be formulated as follows:

$$
\begin{aligned}
\text{minimize} \quad & \left\{ \mu\big[f_i(\mathbf{x},\mathbf{d},\mathbf{p})\big], \upsilon\big[f_i(\mathbf{x},\mathbf{d},\mathbf{p})\big] \right\} \quad (i = 1,2,3,\ldots,k), \\
\text{subject to} \quad & \left\{ P\big[G_j(\mathbf{x},\mathbf{d},\mathbf{p}) \le \varepsilon_j\big] \right\} \quad (j = 1,2,3,\ldots,m), \\
& \mathbf{x}^{(L)} \le \mathbf{x} \le \mathbf{x}^{(U)}, \\
& \mathbf{d}^{(L)} \le \mathbf{d} \le \mathbf{d}^{(U)}.
\end{aligned}
\tag{3.4}
$$

Taking into consideration the stochastic distribution of uncertain parameters, the probability of failure, $P[G(\mathbf{x},\mathbf{d},\mathbf{p}) \le 0]$, can now be evaluated for each probability function as

$$
P_f^i = \int_{G_i(\mathbf{x},\ \mathbf{d},\mathbf{p}) \le 0} f_X(X)dX,
\tag{3.5}
$$

where f_X is the probability density function of $X = (x,p)$. This integral is, in fact, very complicated particularly for systems with complex G_i $(\mathbf{x},\ \mathbf{d},\ \mathbf{p})$ [34], and Monte Carlo simulation is alternatively used to approximate (3.5). In this case, a binary indicator function is defined such that it has the value of 1 in the case of failure $(G_i(\mathbf{X},\mathbf{d}) \le 0)$ and the value of zero, otherwise:

$$
I_{G_i(X,d)} = \begin{cases} 0, & G_i(X,d) > 0, \\ 1, & G_i(X,d) \le 0. \end{cases}
\tag{3.6}
$$

Consequently, the integral of (3.5) can be rewritten as

$$
P_f^i = \int_{G_i(\mathbf{X},\ \mathbf{d}) \le 0} f_X(X)dX = \int_{-\infty}^{\infty} I_{G_i(\mathbf{X},\mathbf{d})} f_X(X)dX.
\tag{3.7}
$$

Based on Monte Carlo simulation [35, 36], the probability using sampling technique can be estimated using

$$
P_f^i = \int_{G_i(\mathbf{X},\ \mathbf{d}) \le 0} f_X(X)dX = \frac{1}{N}\sum_{i=1}^{N} I_{G_i(X,d)}.
\tag{3.8}
$$

In other words, the probability of failure is equal to the number of samples in the failure region divided by the total number of samples. Evidently, such estimation of P_f approaches the actual value in the limit as $N \to \infty$ [34]. However, there have been many research activities on sampling techniques to reduce the number of samples keeping a high level

of accuracy. A newer method that has become more widely used is Hammersley Sequence Sampling (HSS). HSS is considered a quasi-MC sampling method because deterministic points are used instead of random points. Hammersley points are used to divide a unit hypercube, providing uniform sample points across the sample space. Since the points are chosen on a unit hypercube, they are transformed to the given parameter distributions providing sample points for simulation. This method produces good coverage of the distribution with a greatly reduced set of sample points [37–39].

4. Robust Design of the S-Shaped Box Beam

The mathematical model of peak crushing force (P_{max}) obtained in previous section is now employed as model in the reliability-based robust design process. The desired value of P_{max} is considered less than 70 KN due to occupant safety and more than 35 KN due to vehicle safety. Therefore, optimization of the mean value of peak crushing force is not the aim of this paper. The goal of the robust design approach presented in this study is to minimize the variation of P_{max} subjected to probabilistic constraint considering uncertain design variables. This reliability-based robust design process can be formulated as:

$$
\text{minimize } f = \text{ variance-per-mean ratio } \left(\frac{\sigma^2}{\mu} \right) \text{of Peak Crushing Force,}
$$

subject to the reliability-based inequality constraint :

probability of failure of P_{max} : $\text{Pr}_{P\,max} \leq 0.1$,

where $\text{Pr}_{P\,max} = P\ [\ 35\,\text{KN} \leq P_{max} \leq 70\,\text{KN}]$,

$$(4.1)$$

and the deterministic inequality constraints :

$$
R \leq \frac{D}{2(1 - \cos \theta)},
$$

$35° \leq \theta \leq 60°, \ 150\,\text{mm} \leq R \leq 829\,\text{mm}, \ 50\,\text{mm} \leq C \leq 70\,\text{mm},$

$1.5\,\text{mm} \leq t \leq 3\,\text{mm}, \ 150\,\text{mm} \leq D \leq 300\,\text{mm}.$

In the case of robust design, parameters like density and yield stress vary according to a priori known probabilistic distribution functions around a nominal set of parameters. In this study, the uncertain design parameters, namely, σ_0 and t are varied with the Gaussian distributions. The standard deviations of the Gaussian distributions are considered equal to 5.5 and 0.05 for σ_0 and t, respectively.

The evolutionary process of multiobjective optimization is accomplished by 1000 Monte Carlo evaluations using HSS (Hammersley Sequence Sampling) distribution. In the optimization process, the population size, the crossover probability P_c, and the mutation probability P_m are considered equal to 100, 0.7, and 0.07, respectively.

Results have been produced for the S-beams with various values of the offset of two-end parts (D = 150, 200, 250, 300) and various values of the web width (C = 50, 55, 60, 65, 70). In this way, for each specific value of D and C, genetic algorithm is used to find optimal values of other design parameters: R, θ, and t.
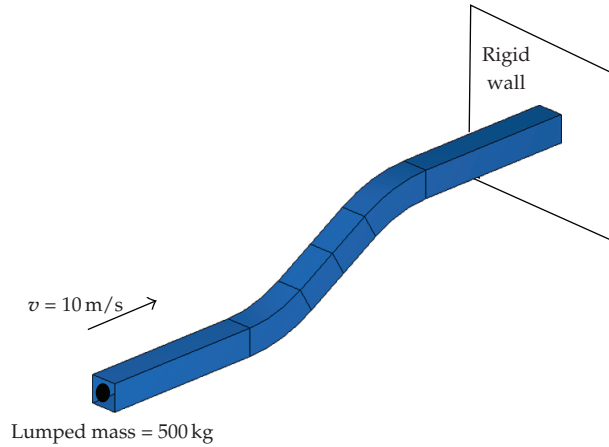
Figure 9: The impact model of the S-shaped box beam with loading and boundary conditions.
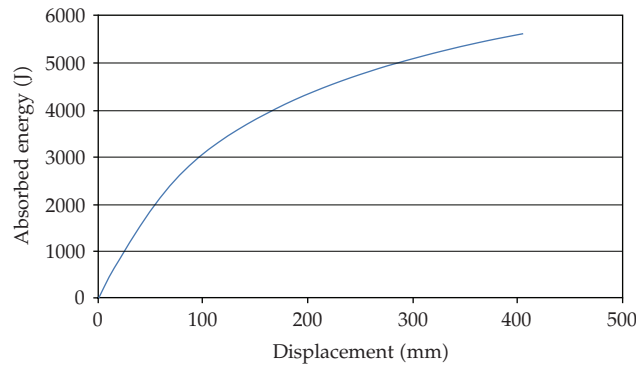

Figure 10: Diagram of the energy absorption during the crushing time for the design point *C1*.

The variance-per-mean ratios of all optimum design points are shown in Table 1. For choosing an optimum design point, additional competing criteria functions such as weight and energy absorption capacity of S-beams are considered as objective functions. In this way, 13 various finite-element analyses have been performed due to those different design points (Table 1) under the same load and boundary conditions. 4-node doubly curved thin-shell elements (S4R) with reduced integration were employed for the finite-element analysis. The material of S-shaped energy absorbers has been considered as elastic-plastic steel with linear strain hardening. The mechanical properties are assumed as follows: Young's modulus $E =$ 206 GPa, Poisson's ratio $\upsilon = 0.3$, plastic modulus $E_T = 1.4$ GPa, yielding stress $\sigma_0 = 162$ MPa, and density $\rho = 7800$ kg/m^3. In order to simulate the dynamic crushing condition, a 500 kg lumped mass with an initial velocity of $V_0 = 10$ m/s is attached to the end of the beam, as shown in Figure 9. The rear end of the beam is considered free just in the direction of impact whilst the front end has been fully clamped.

The computed values of the absorbed energy and the weight of the structure are depicted in Table 1. The results clearly reveal that the designs *B1* and *C1* have maximum absorbed energy and minimum weight, respectively. It is now desired to find a tradeoff optimum design point compromising both objective functions (Absorbed energy & Weight).

Table 1: The values of objective functions and their associated design variables of the obtained design points.

Design	D	C	R	θ	t	Variance-per-mean ratio of	E(J)	W
Point	(mm)	(mm)	(mm)	(deg)	(mm)	P_{max}	(absorbed energy)	(Kg)
A1	150	40	435.11	33.33	3	32.854	4825.93	3.59
A2	150	50	150	60	2.7	35.207	5162.74	4.23
A3	150	60	150	60	2	45.724	4026.45	3.84
A4	150	70	150	60	2	58.996	4507.12	4.5
B1	200	40	571.63	20	3	32.991	5655.6	3.6
B2	200	60	200	60	2.2	41.546	4862.82	4.28
B3	200	70	200	60	2	53.606	4548.25	4.58
C1	250	40	1003.1	22.67	2.9	34.155	5636.96	3.51
C2	250	60	250	60	2.4	39.683	3270.22	4.73
C3	250	70	250	60	2	50.629	2682.26	4.66
D1	300	50	300	22.67	2.3	42.389	5555.49	3.64
D2	300	60	300	60	2.5	37.696	3688.8	5
D3	300	70	300	60	2	48.03	2787.27	4.73

Table 2: The mapped values of objective functions and sum of them for each design point.

Design point	Mapped value of the variance-per-mean ratio of P_{max}	Mapped value of the $(1/E$(J))	Mapped value of the W (Kg)	Sum of the mapped values
A1	0	0.155088883	0.053691	0.20878
A2	0.090008	0.086119127	0.483221	0.659349
A3	0.492311	0.365001847	0.221477	1.07879
A4	1	0.22986911	0.66443	1.894299
B1	**0.005241**	**0**	**0.060403**	**0.065643**
B2	0.332492	0.147068882	0.516779	0.996339
B3	0.793818	0.21963264	0.718121	1.731572
C1	**0.049767**	**0.002983027**	**0**	**0.05275**
C2	0.261227	0.658016681	0.818792	1.738036
C3	0.67994	1	0.771812	2.451752
D1	0.364739	0.016255914	0.087248	0.468243
D2	0.185219	0.480984842	1	1.666204
D3	0.580522	0.928338527	0.818792	2.327652

This can be achieved by the method employed in this paper, namely, the mapping method. In the mapping method, the values of objective functions of all design points are mapped into intervals 0 and 1. Mapped values of each objective function and sum of them are shown in Table 2. Using the sum of the mapped values for each design point, the tradeoff point simply is the one having the minimum sum of those values. Consequently, optimum design point, *C1*, is the tradeoff point which has been obtained from the mapping method. Figure 10 shows
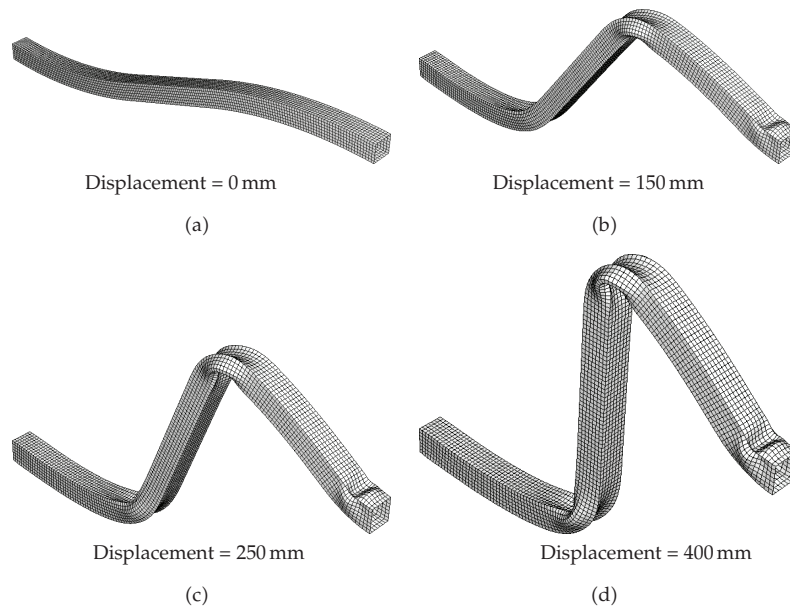
Displacement = 0 mm

(a)

Displacement = 150 mm

(b)

Displacement = 250 mm

(c)

Displacement = 400 mm

(d)

Figure 11: Deformation of optimum design point *C1*.

the diagram of energy absorption during the crushing time for the design point *C1*. The shape of deformation of this design point is shown in Figure 11. These shapes of deformation are at the time when the end displacement reached the values of 150, 250, and 400 mm.

5. Conclusion

An analytical model based on energy method has been employed for the peak crushing force of the S-shaped box beams. Using obtained analytical model and Monte Carlo simulation, genetic algorithm has been used for the robust design of the S-shaped box beams having probabilistic uncertainties in material and geometrical parameters. In this way, 13 design points with minimum variance-per-mean ratio of peak crushing force have been obtained. In order to choose the tradeoff optimum design point, finite-element study using the S4R element using the commercial software *ABAQUS* has been performed and energy absorption capacity of all 13 design points has been computed. The mapping method has been proposed and used in this paper to find the tradeoff optimum design point and one of 13 design points has been chosen using this method. The very good behavior of chosen design point indicates the worthiness of the approach of this paper.

References

[1] A. Pugsley and M. Macaulay, "The large-scale crumpling of thin cylindrical columns," *The Quarterly Journal of Mechanics and Applied Mathematics*, vol. 13, pp. 1–9, 1960.

[2] J. M. Alexander, "An approximate analysis of the collapse of thin cylindrical shells under axial loading," *The Quarterly Journal of Mechanics and Applied Mathematics*, vol. 13, pp. 10–15, 1960.

[3] W. Johnson, *Impact Strength of Material*, Edward Arnold, London, UK, 1972.

[4] N. Jones and W. Abramowicz, "Static and dynamic axial crushing of circular and square tubes," in *Metal Forming and Impact Mechanics*, S. R. Reid, Ed., p. 225, Pergamon Press, Oxford, UK, 1985.

[5] T. Wierzbicki, S. U. Bhat, W. Abramowicz, and D. Brodkin, "Alexander revisited—a two folding elements model of progressive crushing of tubes," *International Journal of Solids and Structures*, vol. 29, no. 24, pp. 3269–3288, 1992.

[6] A. A. Singace, H. Elsobky, and T. Y. Reddy, "On the eccentricity factor in the progressive crushing of tubes," *International Journal of Solids and Structures*, vol. 32, no. 24, pp. 3589–3602, 1995.

[7] N. K. Gupta and R. Velmurugan, "Consideration of internal folding and non-symmetric fold formation in axisymmetric axial collapse of round tubes," *International Journal of Solids and Structures*, vol. 34, no. 20, pp. 2611–2630, 1997.

[8] Y. Ohkami, M. Shimamura, K. Takada, H. Tomizawa, K. Motomura, and M. Usuda, "Collapse of thin-walled curved beam with closed-hat section. Part 1. Study on collapse characteristics," in *Electronic Diesel Engine Controls—Papers Presented at the SAE International Congress and Exposition*, pp. 1–12, Detroit, Mich, USA, March 1990, SAE Paper 900460.

[9] C. M. Ni, "Impact response of curved box beam columns withlarge global and local deformations," in *Proceedings of the 14thStructures, Structural Dynamics, and Materials Conference*, King of Prussia, Pa, USA, 1976, AIAA Paper 73-401.

[10] H.-S. Kim and T. Wierzbicki, "Effect of the cross-sectional shape on crash behavior of a 3-D space frame. Impact and Crashworthiness Laboratory," Tech. Rep. 34, MIT, May 2000.

[11] H.-S. Kim and T. Wierzbicki, "Closed-form solution for crushing response of three-dimensional thin-walled "S" frames with rectangular cross-sections," *International Journal of Impact Engineering*, vol. 30, no. 1, pp. 87–112, 2004.

[12] L. Zheng and T. Wierzbicki, "Quasi-static crushing of S-shaped aluminum front rail," *International Journal of Crashworthiness*, vol. 9, no. 2, pp. 155–173, 2004.

[13] P. Hosseini-Tehrani and M. Nikahd, "Two materials S-frame representation for improving crashworthiness and lightening," *Thin-Walled Structures*, vol. 44, no. 4, pp. 407–414, 2006.

[14] Y. Liu and M. L. Day, "Bending collapse of thin-walled circular tubes and computational application," *Thin-Walled Structures*, vol. 46, no. 4, pp. 442–450, 2008.

[15] A. Jamali, A. Hajiloo, and N. Nariman-zadeh, "Reliability-based robust Pareto design of linear state feedback controllers using a multi-objective uniform-diversity genetic algorithm (MUGA)," *Expert Systems with Applications*, vol. 37, no. 1, pp. 401–413, 2010.

[16] D. Lönn, M. Öman, L. Nilsson, and K. Simonsson, "Finite element based robustness study of a truck cab subjected to impact loading," *International Journal of Crashworthiness*, vol. 14, no. 2, pp. 111–124, 2009.

[17] I. Kucuk, S. Adali, and I. Sadek, "Robust optimal design of beams subject to uncertain loads," *Mathematical Problems in Engineering*, vol. 2009, Article ID 841017, 17 pages, 2009.

[18] G. Augusti, A. Baratta, and F. Casciati, *Probabilistic Methods in Structural Engineering*, Chapman & Hall, London, UK, 1984.

[19] G. Augusti and A. Baratta, "Limit analysis of structures with stochastic strength variation," *Journal of Structural Mechanics*, vol. 1, no. 1, pp. 43–62, 1972.

[20] U. Alibrandi and G. Ricciardi, "The use stochastic stresses in the static approach of probabilistic limit analysis," *International Journal for Numerical Methods in Engineering*, vol. 73, no. 6, pp. 747–782, 2008.

[21] O. Ditlevsen and O. H. Madsen, *Structural Reliability Methods*, John Wiley & Sons, New York, NY, USA, 1996.

[22] H. G. Matthies, C. E. Brenner, C. G. Bucher, and C. G. Soares, "Uncertainties in probabilistic numerical analysis of structures and solids—stochastic finite elements," *Structural Safety*, vol. 19, no. 3, pp. 283–336, 1997.

[23] S. Okazawa, K. Oide, K. Ikeda, and K. Terada, "Imperfection sensitivity and probabilistic variation of tensile strength of steel members," *International Journal of Solids and Structures*, vol. 39, no. 6, pp. 1651–1671, 2002.

[24] C. A. Schenk and G. I. Schuëller, *Uncertainty Assessment of Large Finite Element Systems*, Springer, Berlin, Germany, 2005.

[25] D. Lim, Y. S. Ong, and B. S. Lee, "Inverse multi-objective robust evolutionary design optimization in the presence of uncertainty," in *Proceedings of the Workshops on Genetic and Evolutionary Computation (GECCO '05)*, pp. 55–62, Washington, DC, USA, 2005.

[26] M. Papadrakakis, N. D. Lagaros, and V. Plevris, "Structural optimization considering the probabilistic system response," *International Journal of Theoretical Applied Mechanics*, vol. 31, no. 3-4, pp. 361–393, 34.

[27] J. S. Arora, *Introduction to Optimum Design*, McGraw-Hill, New York, NY, USA, 1989.

[28] S. S. Rao, *Engineering Optimization: Theory and Practice*, John Wiley & Sons, New York, NY, USA, 1996.

[29] N. Amanifard, N. Nariman-Zadeh, M. Borji, A. Khalkhali, and A. Habibdoust, "Modelling and Pareto optimization of heat transfer and flow coefficients in microchannels using GMDH type neural networks and genetic algorithms," *Energy Conversion and Management*, vol. 49, no. 2, pp. 311–325, 2008.

[30] K. Atashkari, N. Nariman-Zadeh, M. Gölcü, A. Khalkhali, and A. Jamali, "Modelling and multi-objective optimization of a variable valve-timing spark-ignition engine using polynomial neural networks and evolutionary algorithms," *Energy Conversion and Management*, vol. 48, no. 3, pp. 1029–1041, 2007.

[31] D. E. Goldberg, *Genetic Algorithms in Search, Optimization, and Machine Learning*, Addison-Wesley, Boston, Mass, USA, 1989.

[32] T. Back, D. B. Fogel, and Z. Michalewic, Eds., *Handbook of Evolutionary Computation*, Institute of Physics Publishing, Bristol, UK; Oxford University Press, New York, NY, USA, 1997.

[33] G. Renner and A. Ekárt, "Genetic algorithms in computer aided design," *CAD Computer Aided Design*, vol. 35, no. 8, pp. 709–726, 2003.

[34] Q. Wang and R. F. Stengel, "Robust control of nonlinear systems with parametric uncertainty," *Automatica*, vol. 38, no. 9, pp. 1591–1599, 2002.

[35] M. H. Kalos and P. A. Whitlock, *Monte Carlo Methods*, Wiley-Blackwell, Weinheim, Germany, 2nd edition, 2008.

[36] Z. Kang, *Robust design of structures under uncertainties*, Ph.D. thesis, University of Stuttgart, 2005.

[37] B. A. Smith, S. P. Kenny, and L. G. Crespo, "Probabilistic parameter uncertainty analysis of single input single output control systems," NASA Report TM-2005-213280, NASA, 2005.

[38] L. G. Crespo and S. P. Kenny, "Robust control deign for systems with probabilistic uncertainty," NASA Report TP-2005-213531, NASA, 2005.

[39] U. M. Diwekar and J. R. Kalagnanam, "Efficient sampling technique for optimization under uncertainty," *AIChE Journal*, vol. 43, no. 2, pp. 440–447, 1997.